Ecosystems
https://doi.org/10.1007/s10021-021-00709-6

Multi-Scale Temporal Patterns in Stream Biogeochemistry Indicate Linked Permafrost and Ecological Dynamics of Boreal Catchments

Alex J. Webster,[1,3]* Thomas A. Douglas,[2] Peter Regier,[4] Mark D. Scheuerell,[5] and Tamara K. Harms[1,6]

[1]*Institute of Arctic Biology, University of Alaska Fairbanks, Fairbanks, Alaska, USA;* [2]*United States Army Cold Regions Research and Engineering Laboratory, Fairbanks, Alaska, USA;* [3]*Department of Biology, University of New Mexico, Albuquerque, New Mexico, USA;* [4]*Pacific Northwest National Laboratory, Richland, Washington, USA;* [5]*U.S. Geological Survey Washington Cooperative Fish and Wildlife Research Unit, School of Aquatic and Fishery Sciences, University of Washington, Seattle, Washington, USA;* [6]*Department of Biology & Wildlife, University of Alaska Fairbanks, Fairbanks, Alaska, USA*

Abstract

Temporal patterns in stream chemistry provide integrated signals describing the hydrological and ecological state of whole catchments. However, stream chemistry integrates multi-scale signals of processes occurring in both the catchment and stream. Deconvoluting these signals could identify mechanisms of solute transport and transformation and provide a basis for monitoring ecosystem change. We applied trend analysis, wavelet decomposition, multivariate autoregressive state-space modeling, and analysis of concentration–discharge relationships to assess temporal patterns in high-frequency (15 min) stream chemistry from permafrost-influenced boreal catchments in Interior Alaska at diel, storm, and seasonal time scales. We compared catchments that varied in spatial extent of permafrost to identify characteristic biogeochemical signals. Catchments with higher spatial extents of permafrost were characterized by increasing nitrate concentration through the thaw season, an abrupt increase in nitrate and fluorescent dissolved organic matter (fDOM) and declining conductivity in late summer, and flushing of nitrate and fDOM during summer rainstorms. In contrast, these patterns were absent, of lower magnitude, or reversed in catchments with lower permafrost extent. Solute dynamics revealed a positive influence of permafrost on fDOM export and the role of shallow, seasonally dynamic flowpaths in delivering solutes from high-permafrost catchments to streams. Lower spatial extent of permafrost resulted in static delivery of nitrate and limited transport of fDOM to streams. Shifts in concentration–discharge relationships and seasonal trends in stream chemistry toward less temporally dynamic patterns might therefore indicate reorganized catchment hydrology and biogeochemistry due to permafrost thaw.

Received 14 October 2020; accepted 15 September 2021

Supplementary Information: The online version contains supplementary material available at https://doi.org/10.1007/s10021-021-00709-6.

Author contributions: AJW, PR, and TKH designed the study. PR and TKH collected the data. AJW, TKH, TAD, and MDS analyzed and interpreted the data. AJW and TKH wrote the manuscript with contributions from all authors.

**Corresponding author; e-mail:* awebster2@unm.edu

Published online: 04 October 2021

Key words: nitrate (NO_3^-); dissolved organic matter (DOM); multivariate autoregressive state-space (MARSS) models; flowpaths; wavelets; concentration–discharge relationships; storms; time series analysis; nitrate isotopes.

Introduction

Temporal patterns in stream chemistry provide integrated signals describing the hydrological and ecological state of whole catchments (Likens and others 1970). Seasonal trends, storm responses, and diel fluctuations in stream chemistry can reveal the distribution of hydrologic flowpaths, dominant biogeochemical processes, and phenology of water and energy exchange within catchments, as well as biotic processes in receiving streams (Kirchner and others 2004; Hall and others 2016; Burns and others 2019). Deviation or long-term change in these characteristic patterns might therefore indicate ecosystem responses to changing climate and disturbance regimes (for example, Czikowsky and Fitzjarrald 2004; Keller and others 2010; Jones and others 2017; Fork and others 2020). However, gaining mechanistic insights from records of stream chemistry requires deconvoluting signals that arise from both terrestrial and aquatic processes and occur on multiple time scales (Bernhardt and others 2005; Brookshire and others 2009).

Stream chemistry in the boreal forest of Alaska reflects the influence of spatially discontinuous permafrost (ground that remains frozen for ≥ 2 years) on hydrological and ecological processes. Forests underlain by permafrost have cold, moist soils and low rates of organic matter decomposition and nutrient cycling (van Cleve and others 1991). Organic matter accumulates on the forest floor where it insulates permafrost, fosters growth of spruce forests, and provides a source of dissolved organic matter (DOM) (Johnstone and others 2010; Jorgenson and others 2010; Ping and others 2010). Ice-rich permafrost confines hydrologic flowpaths to shallow, seasonally thawed soils (the active layer) of relatively high organic content (Haugen and others 1982; Jorgenson and others 2010), resulting in DOM export to streams (Petrone and others 2006; Harms and others 2016). In contrast, permafrost-free soils are warmer and drier and favor establishment of deciduous forests that store organic matter in aboveground biomass, rather than in the forest floor (Johnstone and others 2010; Alexander and Mack 2016). Here, deeper flowpaths through well-drained hillslopes interact with mineral soils and fractured bedrock aquifers (Yoshikawa and others 2003), which support little nitrate (NO_3^-) uptake (Harms and Jones 2012) and are therefore sources of NO_3^- (Verplanck and others 2003).

Permafrost and resulting patterns in forest composition thus impart biogeochemical signals that are transported by hydrologic flowpaths to streams. Identifying the mechanisms that generate temporal patterns in stream chemistry of permafrost-influenced catchments might provide new approaches for tracking catchment-scale permafrost distribution and understanding its influence on ecosystems. Spatially distributed analyses have demonstrated that streams draining catchments of lower permafrost extent or deeper active layer depth have lower DOM and higher NO_3^- concentrations (Petrone and others 2006; Harms and others 2016). These patterns are hypothesized to result from deeper flowpaths intersecting mineral soils, compared to shallow organic soils. On seasonal time scales, this phenomenon could manifest as season-long directional trends in solute concentrations as groundwater flowpaths migrate from organic to mineral layers as the active layer thaws (Harms and Jones 2012; Table 1: H1). During storms, the timing, magnitude, and duration of concentration–discharge relationships could indicate the influence of permafrost on the depth and length of catchment flowpaths as well as the distribution and size of solute pools within catchments (Williams 1989; Petrone and others 2007; Burns and others 2019). For example, where permafrost is present, flowpaths are shallow (Koch and others 2013) and expected to rapidly deliver pulses of DOM from organic-rich soils to streams during storms (Table 1: H2 and H3). Where permafrost is absent, well-drained soils yield longer transit times (Yoshikawa and others 2003) and flowpaths intersect mineral soils, which could produce delayed flushes of inorganic N into streams (Table 1: H2 and H3).

Biotic processes in both streams and catchments also generate temporal signals in stream chemistry. Vegetative uptake regulates NO_3^- export from streams draining nitrogen-limited temperate forests (Likens and others 1970) and could contribute to declines in NO_3^- concentration in streams during periods of peak growth in boreal forests (Table 1: H4). Terrestrial productivity and evapotranspiration can also generate diel variation in stream discharge, flowpath depth, or soil redox conditions that cause corresponding patterns in stream chemistry (Czikowsky and Fitzjarrald 2004; Nimick and others 2011). For example, evapotranspiration

Table 1. Hypothesized Mechanisms Explaining Temporal Patterns in Stream Chemistry of Boreal Catchments that Vary in Spatial Extent of Permafrost.

Hypotheses		Predictions	
H1	*Seasonal* trends in stream chemistry result from deepening of flowpaths as thaw depth increases to encompass mineral soil	P1a	Seasonal increase in NO_3^- concentration (indicator in mineral soil flowpaths) or decline in DOM concentration (indicator in organic soil flowpaths) where permafrost is present
		P1b	No seasonal trends in stream chemistry where permafrost is sporadic
H2	*Within-season* variation in stream chemistry results from mobilization of differential stores of solutes during storms	P2a	Positive correlations between solute concentrations, precipitation, and discharge
		P2b	Flushing of DOM (indicator of large organic solute pool) during storm events where permafrost is present
		P2c	Flushing of NO_3^- (indicator of large inorganic solute pool) during storm events where permafrost is sporadic
H3	*Within-season* variation in stream chemistry results from storm-activated flowpaths	P3a	Clockwise hysteresis of concentration vs discharge during storms (indicator of fast, shallow flowpaths) where permafrost is present
		P3b	Anti-clockwise hysteresis of concentration vs discharge during storms (indicator of transport limitation and slower, deeper flowpaths) where permafrost is sporadic
H4	*Within-season* variation in stream chemistry results from uptake of N by terrestrial vegetation	P4a	Negative correlation of growing degree units (indicator of conditions favorable to terrestrial primary production) with NO_3^- concentration
H5	*Diel* variation in stream chemistry results from the influence of transpiration by terrestrial vegetation on flowpath depth or soil redox conditions	P5a	Diel oscillations in discharge (indicator of evapotranspiration) negatively correlated with NO_3^- and positively correlated with DOM concentration
H6	*Diel* variation in stream chemistry results from uptake and release of C and N by stream biota	P6a	Negative correlation of NO_3^- concentration with PAR or in-stream GPP (indicators of autotropic activity)
		P6b	DOM concentration positively correlated with PAR or in-stream GPP and/or negatively correlated with in-stream ER (indicator of biotic processing of organic carbon)

NO_3^- nitrate.
DOM Dissolved organic matter, GPP gross primary productivity, ER Ecosystem respiration

during the day can lower water tables and promote nitrification by oxygenating soils (Duncan and others 2015). At night, a higher water table might foster denitrification and decreased NO_3^- export (Flewelling and others 2013) or elevate DOM export as shallower flowpaths intersect organic-rich soils. Such patterns caused by terrestrial productivity would result in synchronous diel changes in stream discharge and chemistry (Table 1: H5). Alternatively, diel patterns might arise from metabolism in streams, whereby primary producers draw down NO_3^- concentration and release DOM during daytime (Odum 1956; Nimick and others 2011; Hall and others 2016). Biogeochemical signals imparted by in-stream biota would therefore occur in synchrony with aquatic photosynthesis and respiration (Table 1: H6). Such biotic-driven patterns could vary with permafrost and forest composition or may need to be disentangled from stream chemistry records to identify other signals.

We examined the temporal patterns in catchment biogeochemistry emerging from catchments varying in spatial extent of permafrost. We collected high-frequency (15 min) records of stream chemistry using sensors deployed in four headwater boreal catchments and used these data to test hypotheses regarding the processes generating temporal patterns and how they related to permafrost extent (Table 1). Specifically, we tested hypotheses distinguishing signals generated in

catchments from those produced within streams at seasonal (H1), within-season (H2–H4), and diel time scales (H5–H6) using statistical approaches to deconvolute temporal patterns into characteristic frequencies and assess correlations of biogeochemical patterns with potential drivers.

Methods

Site Description

We monitored four headwater streams in the Caribou-Poker Creeks Research Watershed (CPCRW), which is part of the Bonanza Creek Long-Term Ecological Research Program in the boreal biome of Interior Alaska. Mean annual air temperature is –3.6°C, with the lowest mean monthly temperature typically in January (–23.2°C) and highest in July (15.1°C). During the study period (May–Sept 2017), mean monthly temperatures were similar to long-term averages, with the exception of mean July temperatures approximately 2°C warmer than average. The CPCRW receives 351-mm precipitation annually on average, with 294 mm falling as rain. Mean monthly precipitation during the study period was higher in May (39.4 compared with 24.5 mm), lower in June (34.8 compared with 57.9 mm), and similar in July (104 compared with 96.9 mm) and August (83.1 compared with 82.0 mm) compared to long-term monthly averages.

In the study area, thin (approximately 1 m) soils are underlain by a fractured bedrock aquifer of weathered schist, dispersed carbonate-bearing lithologies, bands of gravel and loess, and spatially discontinuous permafrost (Haugen and others 1982; Yoshikawa and others 2003). Permafrost underlies valley bottoms and north-facing slopes. North-facing slopes are dominated by black spruce (*Picea mariana*) with mosses in the understory (for example, *Sphagnum* spp., *Hylocomium* spp.). South-facing slopes and ridges are dominated by mixed hardwoods (*Betula neoalaskana* and *Populus tremuloides*) and develop little understory groundcover.

The monitored streams drain catchments of varying aspect and therefore spatial extent of permafrost (Figure 1). Though aspect is not replicated, the study design captured a gradient in permafrost extent from minimal to nearly spatially continuous permafrost extent within the drainage network of each catchment. A south-facing catchment (C2, hereafter ''low permafrost'') is underlain by permafrost in approximately 4.5% of its total area and 10% of its drainage network area, defined as the stream network and likely areas of zero-order channels and shallow subsurface flow (see Appendix 1: *Geospatial analysis*). A southeast-facing catchment (C4; hereafter ''low-mid-permafrost'') is underlain by permafrost in 25% of its total area and 30% of its drainage network area. In contrast, a northwest-facing catchment (P6; hereafter ''mid-permafrost'') is underlain by permafrost in 38% of its total area and 66% of its drainage network area, and a north-facing catchment (C3; hereafter ''high permafrost'') is underlain by permafrost in 57% of its total area and 97% of its drainage network area. The catchments also vary in fire history. An experimental fire burned 28% of the C4 catchment in 1999 (Hinzman and others 2003) and a wildfire burned 65% of the P6 catchment in 2004 (Betts and Jones 2009). Streams draining catchments are narrow (< 1 m width) and have closed canopy or are well shaded (Betts and Jones 2009; Mutschlecner and others 2018).

Data Collection

We installed in situ sensors adjacent to an existing flume for gauging discharge in each catchment and monitored stream chemistry at 15 min frequency from May 23–Aug 31, 2017 (Figure 1). We instrumented the high- and low-permafrost catchments with a Submersible Ultra-Violet Nitrate Analyzer (SUNA, Satlantic LP, Seabird Scientific, Halifax, NS, Canada) to measure NO_3^- concentration (LOQ = 0.014 mg N l^{-1}, short-term precision = 0.004 mg N l^{-1}). Nitrate and organic N comprise the majority of dissolved N in the study streams and contribute nearly equally to total N loads, on average (Petrone and others 2006). We instrumented all four streams with photosynthetically active radiation (PAR) loggers (Odyssey, Christchurch, New Zealand) at water level and EXO2 multi-parameter water quality sondes (YSI, Yellow Springs, OH, USA) equipped to measure fluorescent dissolved organic matter (fDOM), turbidity, specific conductivity (SPC), and temperature. The EXO sondes installed in the high- and low-permafrost catchments were additionally equipped with optical dissolved oxygen (DO) sensors. Before deployment, we verified that SUNAs met the manufacturer specification of $\pm$ 0.028 mg N l^{-1} in nanopore water and we calibrated SPC, fDOM, and turbidity sensors to externally-verified standards. Following manufacturer's specifications, we calibrated DO sensors in moist air. Once deployed, we recalibrated all EXO sensors monthly, checked EXO and SUNA sensors against nanopure water for drift and biofouling weekly, and cleaned optical read windows weekly. Sensors collected a

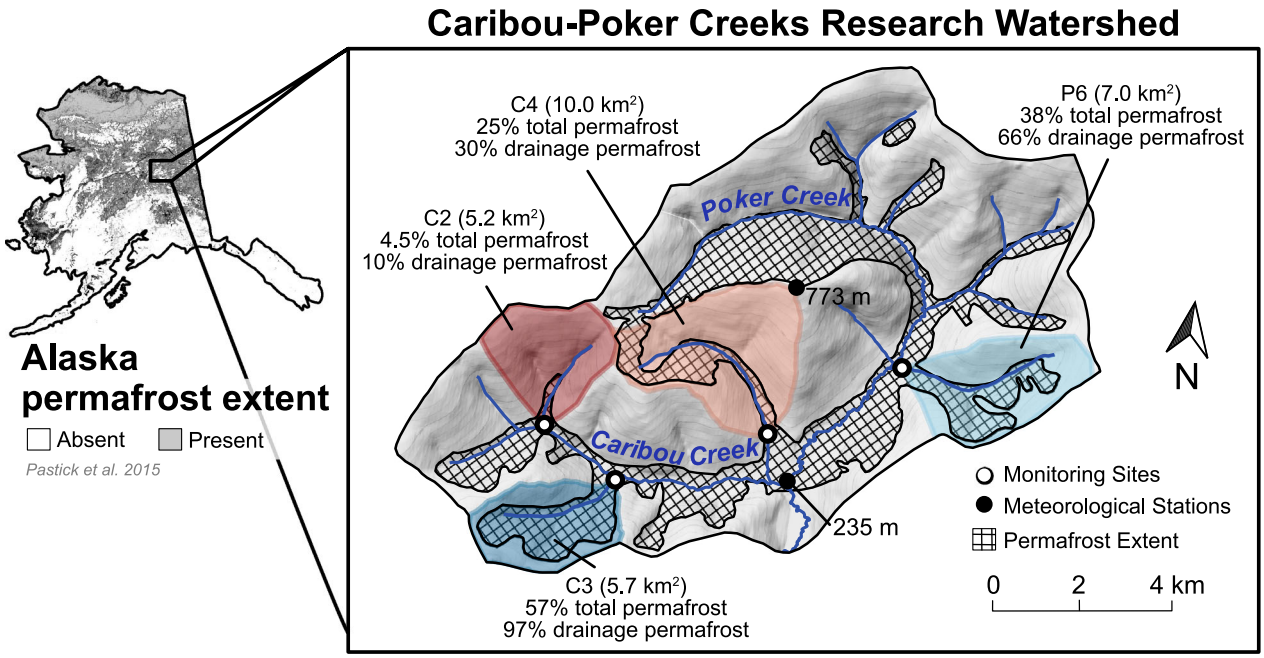

Figure 1. Study catchments within the Caribou-Poker Creeks Research Watershed in the boreal biome of Interior Alaska, USA, where permafrost is discontinuously distributed. The four headwater streams included in the study drain catchments varying in the spatial extent of permafrost, indicated for both the whole catchment (% total permafrost) and the catchment drainage network area (% drainage permafrost).

burst of 9–15 measurements within 30 s at each 15-min interval, and the mean and variance of these measurements were used to detect faulty measurements and estimate uncertainty in subsequent analyses.

Water samples were collected weekly for validation of sensor data. Water samples were filtered in the field (0.7-µm glass fiber filters), transported on ice to the laboratory, and frozen until analysis. Nitrate was analyzed by ion chromatography on a Thermo ICS-2100 with AS-18 columns (LOQ = 0.0017 mg N l^{-1}). Dissolved organic carbon (DOC) was analyzed on a Shimadzu Total Carbon analyzer by combustion followed by non-dispersive infrared gas analysis (LOQ = 8 µM). NO_3^- concentration measured by each SUNA was corrected to laboratory-measured values with site-specific calibration curves (low-permafrost n = 11, slope = 0.94 [95% CI = 0.56, 1.32], R^2 = 0.75; high-permafrost n = 12, slope = 0.91 [95% CI = 0.82, 1.01], R^2 = 0.98). EXO-measured fDOM was corrected for temperature and turbidity as described in Watras and others (2011) and Downing and others (2012). Corrected fDOM concentration was correlated with lab-determined DOC concentration across all sites (R^2 = 0.67, n = 30). However, the strength of this relationship varied among sites (site-specific R^2 range = 0.029–0.95) and we report fDOM in quinine sulfate units (QSU).

We gathered hydrological and meteorological attributes (lter.uaf.edu/data) to evaluate the influence of storms (Table 1: H2–H3) and terrestrial primary productivity (Table 1: H4) on stream chemistry. First, discharge was monitored using pressure transducers installed at flumes adjacent to sensor installations in each catchment. In-stream pressure was corrected for barometric pressure and converted to discharge with rating curves calculated from weekly measurements of discharge by salt dilution. Second, we obtained hourly precipitation and air temperature data from high- and low-elevation meteorological stations in the CPCRW (Fig. 1) and used mean values of the two stations. We calculated daily growing degree units (GDU), which quantify heat accumulation above a threshold temperature (5°C for boreal regions following Ruosteenoja and others (2016) and references therein). GDU (estimated as $[(Temp._{MAX} + Temp._{MIN}) * 2^{-1}] - 5°C$) were used to approximate growing conditions for terrestrial vegetation and provided a proxy for terrestrial productivity (Bugmann and others 2001; Ueyama and others 2013; Rollinson and others 2017).

To evaluate potential changes in the sources of water and NO_3^- coincident with seasonal migration of flowpaths (Table 1: H1), we compared the isotopic composition of NO_3^- ($\delta^{15}N$ and $\delta^{18}O$) and water ($\delta^{18}O$) in streams to previously observed values in groundwater and precipitation (lter.-uaf.edu/data; T. Douglas, unpublished data). Stable isotopes of NO_3^- were measured using the denitrifier method (Casciotti and others 2002) at the UC Davis Stable Isotope Facility. Ratios of ^{15}N:^{14}N and ^{18}O:^{16}O are reported relative to N_2 in air for $\delta^{15}N_{NO3}$ and to Vienna Standard Mean Ocean Water for $\delta^{18}O_{NO3}$ with analytical precision of ± 0.4‰ for $\delta^{15}N$ and ± 0.5‰ for $\delta^{18}O$. Samples with NO_3^- concentration $<<$ 0.02 mg N l^{-1} were below the LOQ and could not be analyzed. Isotopic composition of H_2O was measured by Cavity Ringdown Spectroscopy on a Picarro L2120i and is reported relative to Vienna Standard Mean Ocean Water with an analytical precision of ± 0.2‰ for ^{18}O.

Statistical Analysis

To test hypotheses linking stream chemistry to ecological and hydrologic processes influenced by permafrost, we examined temporal patterns at diel to seasonal time scales. We assessed seasonal trends (Table 1: H1) and correlates of daily variation in solute chemistry (Table 1: H2–H4) using autoregressive state-space models. Storm-scale analysis of concentration–discharge relationships tested hypotheses regarding the influence of permafrost on solute supplies (Table 1: H2) and depth of hydrologic flowpaths (Table 1: H3). Finally, wavelet decomposition was applied to evaluate the relative magnitude of temporal variation across scales and coherence of solute chemistry with processes occurring within the catchment (Table 1: H5) or stream (Table 1: H6). To facilitate analyses of time series, gaps of less than 24 h were filled by applying a Kalman filter to forecasts from an ARIMA model. All data analyses were performed in R version 4.0.2 (R Core Team 2020).

Stream metabolism—To test possible effects of in-stream biotic processes on stream chemistry (Table 1: H6), we modeled rates of gross primary productivity (GPP) and ecosystem respiration (ER). We used the BAyesian Single-station Estimation of Metabolism (BASEmetab) package (Grace and others 2015; Giling and Bond 2020) because it provides both daily and instantaneous GPP and ER rates and we required instantaneous rates for testing hypotheses about diel variation in stream chemistry. Details related to metabolism model fitting and validation are provided in Appendix 2: *Stream metabolism*.

Seasonal and within-season dynamics—We tested hypotheses explaining variation in stream chemistry at seasonal (Table 1: H1) and within-season (Table 1: H2–H4) time scales using univariate and multivariate autoregressive state-space (MARSS) models, respectively (Holmes and others 2018). The MARSS framework partitions variation among observation error, autoregressive processes, and covariate effects when included. First, to test the hypothesis that seasonal deepening of flowpaths influences stream chemistry where permafrost was present (Table 1: H1), we evaluated season-long trends in stream solutes by fitting univariate autoregressive state-space models to solute concentrations summarized by weekly means. Weekly means reduced the effect of autocorrelation but still captured season-long trends. We fit models to datasets reflecting three different time periods: (a) the longest available time series for each variable in each catchment, (b) excluding the influence of snowmelt (dates < June 15), and (c) excluding a sudden change in discharge and chemistry that occurred in some catchments in late summer (dates > Aug. 14). See Appendix 3: *MARSS models* for details on model selection and fit.

To test hypotheses linking stream chemistry to storm-driven, terrestrial, and in-stream processes (Table 1: H2–H6), we used multivariate models to quantify correlations between NO_3^- or fDOM concentration and covariates reflecting these hypothesized processes. Daily mean values were $\log_{10}$-transformed, centered, and standardized (mean = 0, standard deviation = 1) to meet model assumptions and facilitate comparison of covariate effects. Precipitation was evaluated as a covariate capturing storm effects (Table 1: H2–H3) and was included as total precipitation on the same day as measured stream chemistry as well as lagged by one day because discharge can lag precipitation by 4–48 h (McGuire and McDonnell 2006; Koch and others 2013). The potential effect of terrestrial primary production (Table 1: H4) was evaluated by inclusion of GDU lagged by one day as a covariate. Potential influence of in-stream processes on solute concentrations (Table 1: H6) was quantified by estimating effect sizes associated with daily max PAR and mean GPP and ER. Models also accounted for a sudden change in discharge and chemistry that occurred in some catchments by including a dummy variable corresponding to Aug 14–15. Covariates were uncorrelated with one another (Pearson's $r < |0.4|$). Additionally, GDU, GPP, ER, and precipitation were uncorrelated with day of

year (Pearson's $r < |0.4|$), whereas PAR was negatively correlated. We fit a separate multi-state model for each response variable (NO_3^- or fDOM concentration) and used the longest available time series for each combination of response and covariate data. In-stream GPP and ER were available only for the high- and low-permafrost catchments in June and July. Thus, we explored these potential in-stream effects by fitting a second set of models to the shorter time series. For all models, we tested the hypothesis that each catchment represented a unique ecosystem state by comparing AIC scores of multi-state models to a model representing all catchments as a single state. Further details on fitting multivariate MARSS models are provided in Appendix 3: *MARSS models*.

Storm-scale dynamics—To test hypotheses related to the pool sizes of solutes available for transport to streams (Table 1: H2) and the activation of flowpaths (Table 1: H3) during storms, we analyzed storm-scale concentration–discharge relationships. This analysis entailed delineating individual storms and identifying the rising and falling limbs of discharge responses to precipitation. Discharge in streams draining the high- and mid-permafrost catchments (Figure 1) responded strongly to precipitation, whereas responses in the low- and low-mid-permafrost catchments were subtle. However, solute concentrations responded to precipitation in all catchments. We identified storms as events when discharge exceeded 41.9 L s^{-1} and 64.3 L s^{-1} in the high- and mid-permafrost catchments, respectively. These thresholds correspond to twice the mean base flow for each catchment, which we calculated using a recursive digital filter approach from the EcoHydRology package (Fuka and others 2018). In catchments with weak discharge responses, we identified storms within the time windows of events identified in the nearest ''responsive'' catchment, rather than using a discharge threshold. In all catchments, we delineated the beginning of each storm as the inflection point when discharge began to rise and the end point when discharge returned to the pre-event level or when another storm began.

To compare storm dynamics across catchments and events, we calculated a hysteresis index (HI) and flushing index (FI) for NO_3^-, fDOM, turbidity, and SPC during each storm (Lloyd and others 2016; Vaughan and others 2017). The HI indicates the magnitude and direction of hysteretic responses of solute concentration to rising and falling discharge and was calculated at every 2% interval of normalized discharge of each event. The HI at each Q interval i was calculated as $HI_i = C_{RL} - C_{FL}$ where C_{RL} and C_{FL} are normalized concentrations on the rising and falling limb, respectively. The median of all HI_i summarizes the central tendency for each event and bootstrapped 95% CIs around the median HI describe uncertainty. Median HI values range between -1 and 1, with negative and positive values indicating anti-clockwise and clockwise hysteresis, respectively. The FI quantifies solute dilution or flushing during each storm as the difference between mean solute concentration at the onset of an event compared to peak discharge. Mean solute concentrations at storm onset and at peak discharge were calculated as the mean of the burst of measurements (n = 9–15 within 30 s) collected by the sensor at each time point. Bootstrapped 95% CI of the difference between these means provided an estimate of uncertainty for each FI.

Multi-scale temporal variation—We conducted complementary analyses in the frequency domain to characterize the relative variation in NO_3^- and fDOM concentrations across time scales and quantify correlations with indicators of terrestrial and in-stream processes (Table 1: H2–H6). Using wavelet analysis, we decomposed 15-min resolution time series into power spectra across a range of frequencies (0.25–32 d), quantifying power as the squared amplitude of oscillations localized in time. We used a 'morlet' mother wavelet, executed with the WaveletComp package (Roesch and Schmidbauer 2018) and determined the significance of wavelet power using an autoregressive (''red'') background noise spectrum and 100 simulations. Wavelet analysis requires continuous time series and datasets with more than 12 h gaps were therefore analyzed separately. We used wavelet coherence to quantify correlations between NO_3^- or fDOM concentrations and indicators of storms (Table 1: H2), terrestrial processes (Table 1: H5), or in-stream processing (Table 1: H6). Wavelet coherence is a measure of localized correlation and phase angles between time series across time–frequency space. Phase angles are in the interval $[-\pi, \pi]$ and describe whether two time series at a given frequency oscillate in synchrony (in-phase = absolute values less than $\pi/2$, for example, NO_3^- is high when discharge is high), anti-synchronously (out-of-phase = absolute values greater than $\pi/2$, for example, NO_3^- is high when discharge is low), while the sign of the phase angle describes which time series is leading in the relationship (Roesch and Schmidbauer 2018).

Results

Seasonal Dynamics

Yields of NO_3^- and fDOM contrasted among catchments at a seasonal timescale (Figure 2). The high-permafrost catchment (C3) exported 32% less NO_3^- and 75% more fDOM, on average, than the low-permafrost catchment (C2; Figure 2). The low-mid-permafrost catchment (C4) exported the least fDOM of all catchments studied, and the mid-permafrost catchment (P6) exported the most (Figure 2).

A season-long, positive trend in NO_3^- concentration occurred in the high-permafrost catchment, consistent with the prediction that a seasonal increase in NO_3^- concentration would occur where permafrost is present (Table 1: H1-P1a; Figure 3). The positive trend was significant both before (0.007 mg N l^{-1} wk^{-1}, 95% CI: 0.001–0.01) and including a rapid increase in NO_3^- concentration that occurred late in the monitoring period (0.02 mg N l^{-1} wk^{-1}, 95% CI: 0.002–0.03), and also when the snowmelt period prior to June 15 was excluded (0.02 mg N l^{-1} wk^{-1}, 95% CI: 0.0002–0.04). No other measured solutes exhibited significant trends in any catchment (Table S1).

A rapid sustained increase in discharge and solute concentrations punctuated the seasonal records of the high- and mid-permafrost catchment. In the high-permafrost catchment, this ''step-change'' entailed an increase of about 0.2 mg NO_3^--N l^{-1} starting on Aug 14 that was sustained through the remaining period of monitoring (Figure 3). The increase in NO_3^- concentration was accompanied by increased discharge and a decline in SPC, though the increase in NO_3^- concentration was disproportionately large (fDOM data were unavailable in this catchment during this period; Figure 3). A similar increase in NO_3^- concentration was observed in weekly samples in the mid-permafrost catchment and was accompanied by a sustained increase in fDOM of about 6 QSU (Figure 3). Analogous patterns were not observed in the low- or mid-low-permafrost catchment.

The step-change in solute concentrations was accompanied by a change in isotopic composition of NO_3^- (Figure 4). In general, $\delta^{18}O_{NO3}$, $\delta^{15}N_{NO3}$, and $\delta^{18}O_{H2O}$ of streams were bounded by values observed in groundwater from springs and wells, and the range of $\delta^{18}O_{H2O}$ values we observed were similar to those observed in the nearby Nome Creek catchment (Koch and others 2014). Stream $\delta^{15}N_{NO3}$ significantly increased after the step-change by 0.71‰ and 1.35‰ in the high- and mid-permafrost catchments, respectively (Figure 4), as indicated by non-overlapping bootstrapped 95% CIs of mean values before and after the step-change. Similarly, mean stream $\delta^{18}O_{NO3}$ significantly increased across the same catchments and dates by 0.83‰ and 0.79‰ in the high- and mid-permafrost catchments, respectively. Stream $\delta^{18}O_{NO3}$ and $\delta^{15}N_{NO3}$ in catchments where no step-change occurred and $\delta^{18}O_{H2O}$ in all catchments showed little seasonal variation (Figure 4).

Within-Season Dynamics

Daily variation in stream chemistry within the period of measurement was strongly correlated with precipitation, as indicated by significant covariate effects in MARSS models. NO_3^- and fDOM concentrations were significantly correlated with same-day and/or the previous-day precipita-

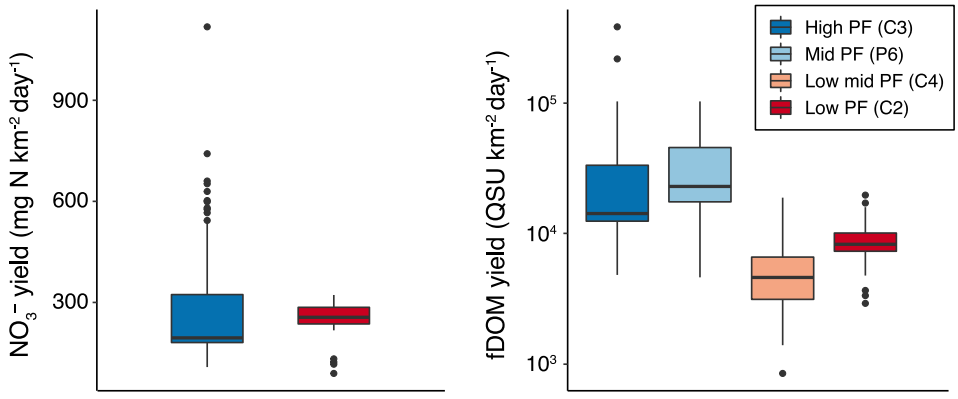

Figure 2. Daily yields of NO_3^- and fDOM from catchments with varying permafrost extent (PF) summarized from 15-min observations collected May–Sept 2017. Center line in boxplot is the median, boxes encompass 25th and 75th percentiles, whiskers are 1.5 × the interquartile ranges, and points reflect values beyond this range. fDOM units are quinine sulfate units (QSU) where 1 QSU = 1 ppb quinine sulfate.

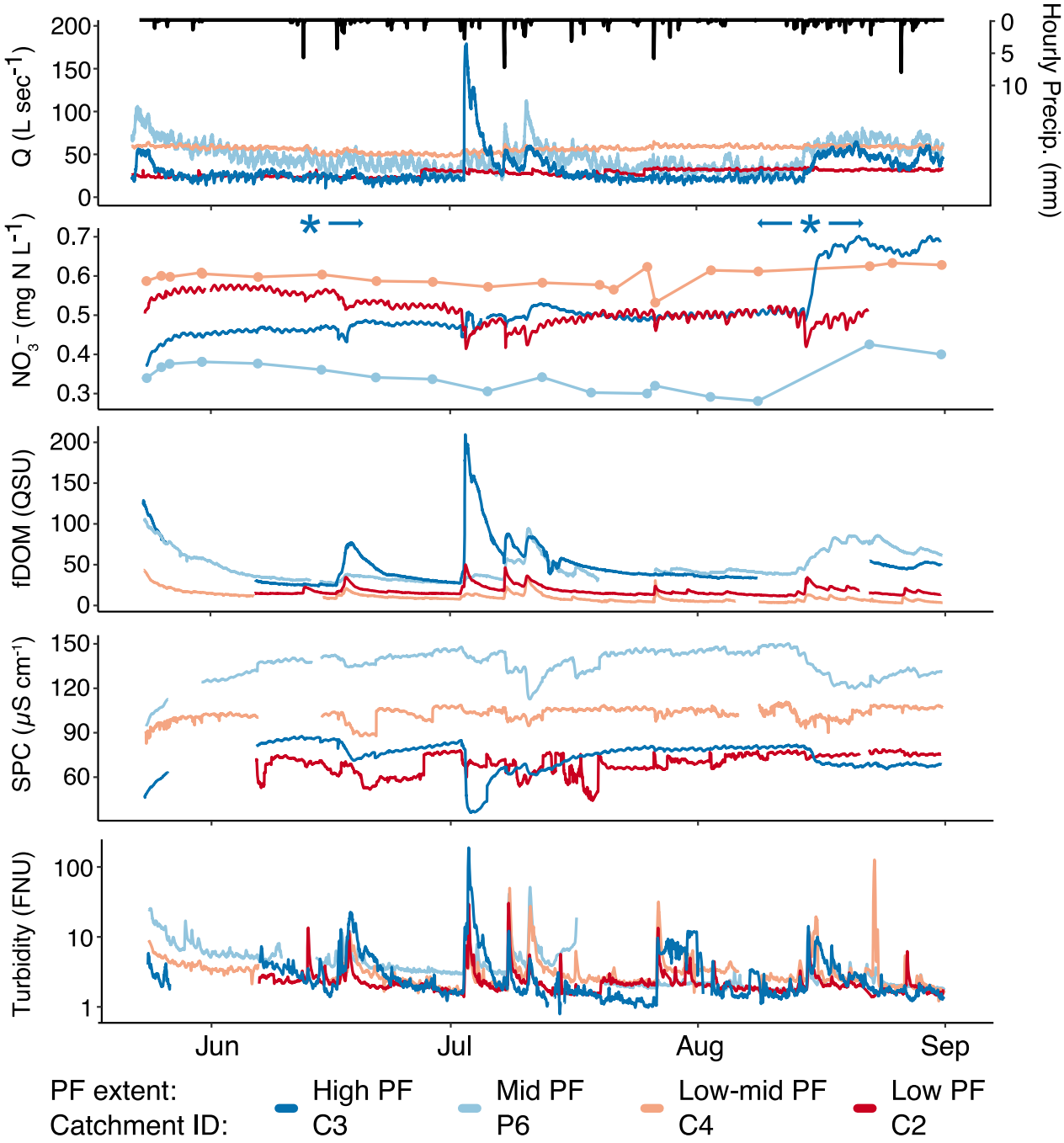

Figure 3. Time series from four streams draining catchments of varying permafrost extent (PF) in 2017. NO_3^- concentration time series include high-frequency observations made by an in-stream sensor in C2 and C3, and weekly grab samples in C4 and P6. ''*'' indicates a significant positive trend in NO_3^- concentration in the high-PF catchment (C3), with arrows indicating significance of the trend before and including the period of Aug. 14–31, as well as when excluding the snowmelt prior to June 15. Q: discharge; NO_3^-: nitrate; fDOM: florescent dissolved organic matter; SPC: specific conductivity.

tion in all catchments (Figure 5A–F). Previous-day precipitation had a strong positive effect on NO_3^- concentration in the high-permafrost catchment (Figure 5A). However, both same- and previous-day precipitation had strong negative effects on NO_3^- concentration in the low-permafrost catchment (Figure 5B), a pattern counter to that predicted to result from larger stores of mobilizable NO_3^- where permafrost is absent (Table 1: H2-P2c). Finally, same- and previous-day precipitation were

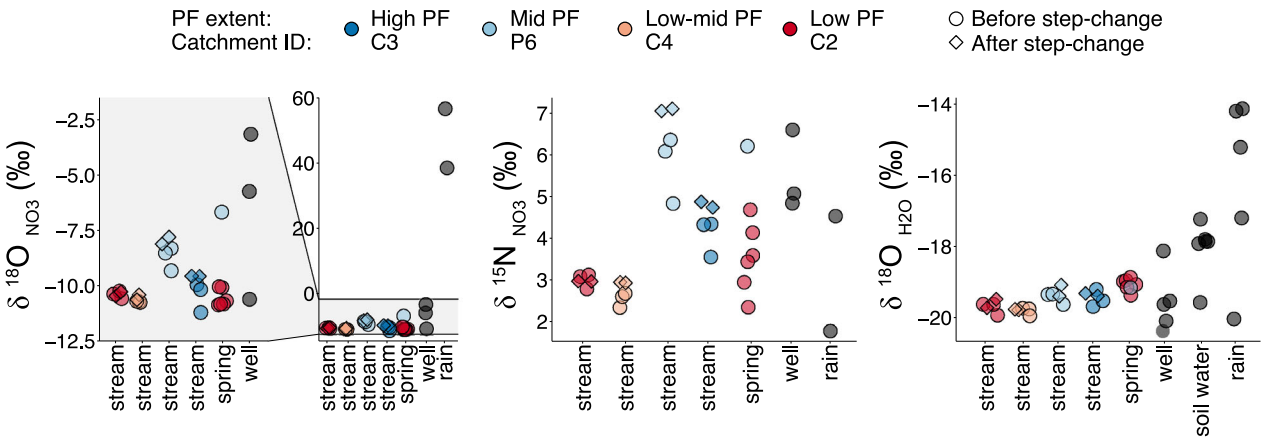

Figure 4. Stable isotopes of NOFor Peer Review 3 – (δ^{18}O and δ^{15}N) and water (δ^{18}O) in the study streams in summer 2017 compared to potential source waters: springs and soil water (note the NO_3^- concentration in soil water was less than required for analysis of NO_3^- isotopes) from the CPCRW, deep groundwater, and rain from the CPCRW and region. Sample dates for source waters range from 2009–2017. Step-change refers to a large increase in NO_3^- concentration that occurred in August 14–15 in the high-permafrost (PF) catchment (C3, dark blue). A similar increase was observed in weekly samples in the mid-permafrost catchment (P6, light blue). No step-change occurred in the low- or low-mid-permafrost catchment (C2 and C4, red and orange). Stream and spring samples are colored by the catchment of origin. Soil water was sampled from the valley bottom near the confluence of Poker and Caribou Creeks (Fig. 1), rain samples are from the low-elevation meteorological station (Fig. 1) and region, and well samples are from regional wells.

positively correlated with fDOM in all catchments (Figure 5C–F), which is also inconsistent with the hypothesis that differential stores of soil OM would result in contrasting temporal dynamics among catchments (Table 1: H2-P2b).

Solute concentrations were also correlated with indicators of in-stream and catchment biological activity on a daily timescale. NO_3^- concentration was negatively correlated with previous-day growing degree units (GDU), an indicator of terrestrial productivity, in both the high- and low-permafrost catchments; this was a predicted result of the hypothesis that uptake of N by terrestrial vegetation influences temporal patterns of NO_3^- concentration in streams (Table 1: H4; Figure 5A–B). GDU was not correlated with fDOM concentration (Figure 5C–F). NO_3^- concentration was also negatively correlated with in-stream GPP in the high-permafrost catchment (Figure S2a), consistent with the predicted result of biotic retention of NO_3^- within streams (Table 1: H6; Figure 5A–B). fDOM concentration was positively correlated with PAR in the low-permafrost catchment and low-mid-permafrost catchments (Figure 5D–F), a pattern suggestive of the role of in-stream production in generating DOM (Table 1: H6). In the high-permafrost catchment, fDOM was negatively correlated with in-stream ER (Figure S2c), providing mixed support for the role of in-stream biota in generating temporal patterns in DOM (Table 1: H6). In all MARSS models, estimating a unique state process for each catchment improved model fit ($AIC_{single\text{-}state} >> AIC_{multi\text{-}state}$), indicating statistically distinguishable temporal patterns among the headwater catchments.

Storm-Scale Dynamics

Storm dynamics indicated differential patterns of solute sources and transport across catchments varying in spatial extent of permafrost (Figure 6). In the high-permafrost catchment, four of five storms resulted in increased NO_3^- concentration (positive FI) and counterclockwise hysteresis (negative HI; Figure 6B). The smallest increase occurred during the first storm observed (July 2), which was followed by dilution of NO_3^- (negative FI) during the next storm (July 7) and flushing of NO_3^- during all storms thereafter (Figure 6B). In the low-permafrost catchment, all storms resulted in dilution of NO_3^-, and all but one storm produced clockwise hysteresis (positive HI; Figure 6B). These patterns are opposite to those predicted to result from larger stores of NO_3^- in deep, permafrost-free soils (Table 1: H2). Though all catchments and storms resulted in flushing of fDOM, only the low- and low-mid-permafrost catchment produced clockwise hysteresis for fDOM. This pattern is opposite of that expected if shallow flowpaths dominate during storms of high, but not low spatial extent of permafrost (Table 1: H3). Temporal dynamics of SPC and turbidity were similar across

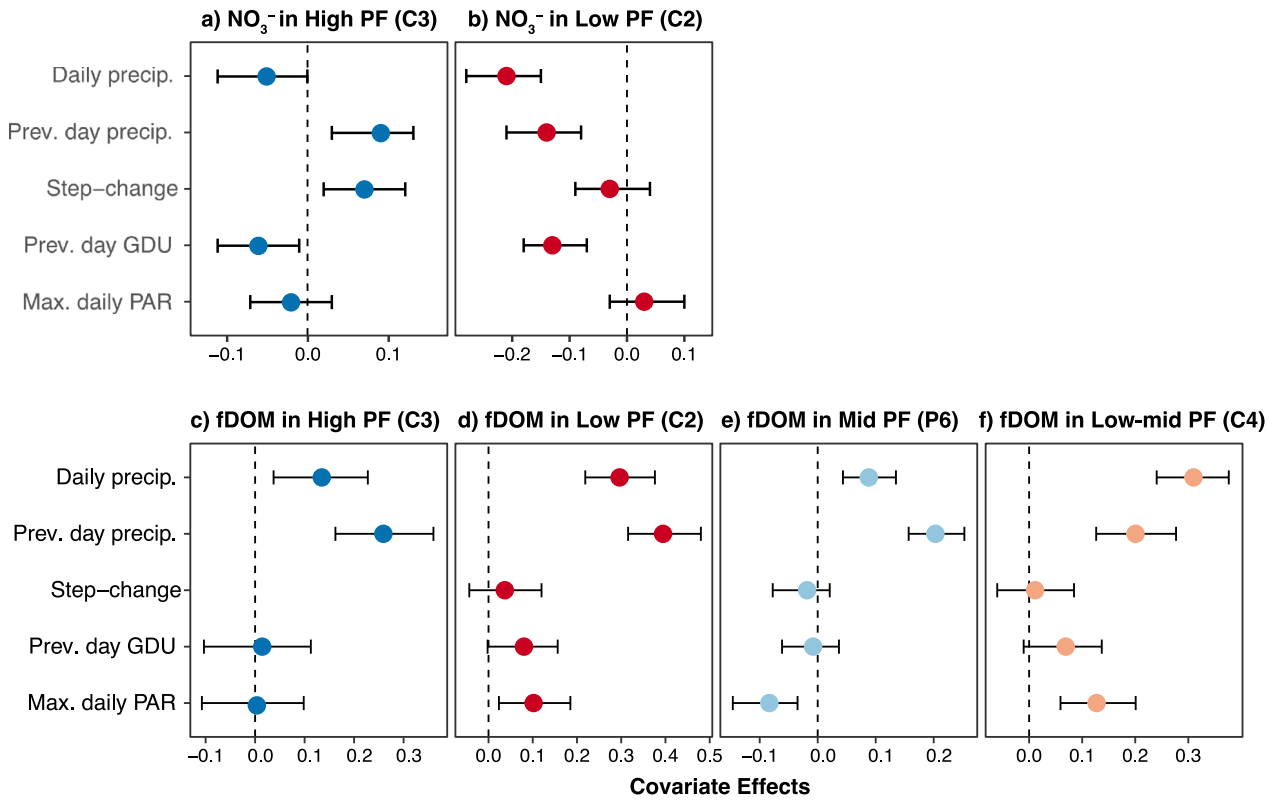

Figure 5. Effects of mean daily precipitation, previous-day precipitation, previous-day growing degree units (GDU), and maximum daily photosynthetic active radiation (Max daily PAR) on mean daily NO_3^- (**A–B**) and fDOM (**C–F**) concentrations in streams draining catchments with varying permafrost extent (PF). Step-change is the effect of a dummy variable used to represent a sudden change in discharge and stream chemistry that occurred in Aug 14–15 in some catchments. Data were centered and standardized. Points are maximum likelihood estimates for effects of covariates on each response variable. Horizontal bars are bootstrapped 95% confidence intervals; bars crossing the vertical dashed line (zero) indicate lack of significance.

all catchments, with dilution and clockwise hysteresis of SPC in nearly all storms (Figure 6D) and heterogeneous patterns in turbidity across storms (Figure 6E).

Multi-Scale Temporal Variation

Wavelet analysis corroborated the significant influence of storms and discharge variation on NO_3^- and fDOM concentrations previously described in the time domain. At frequencies of 2−8 d and times corresponding to storms, oscillations of NO_3^- and fDOM were significantly greater than expected of an autoregressive (red noise) spectrum in all catchments (Figures S3, S4). In the high-permafrost catchment, NO_3^- concentration was coherent with discharge at temporal frequencies and times associated with storms, typically varying in-phase with NO_3^- following discharge (Figure 7A–B), a pattern indicating flushing of NO_3^- during storms and which contradicts the prediction that NO_3^- flushing would only occur where there were larger stores of NO_3^- in deep, permafrost-free soils (Table 1: H2). NO_3^- concentration was also coherent and in-phase with discharge at 4−16 d frequencies during the time period of the step-change in the high-permafrost catchment. At a diel frequency, NO_3^- concentration was coherent with discharge in both the high- and low-permafrost catchments, as predicted to result from the influence of terrestrial transpiration (Table 1: H5). Out-of-phase coherence with NO_3^- leading discharge tended to occur at the diel scale in the high-permafrost catchment during the early thaw season, whereas NO_3^- varied in-phase, following discharge during the later season in the high-permafrost catchment and throughout the record in the low-permafrost catchment (Figure 7A–B). This corresponded to discharge peaks at ∼ 03:00 and NO_3^- peaks at ∼ 04:00 throughout the records of both catchments, with the exception of NO_3^- peaks at ∼ 07:00 in the early thaw season of the high-permafrost catchment. During inter-storm periods,

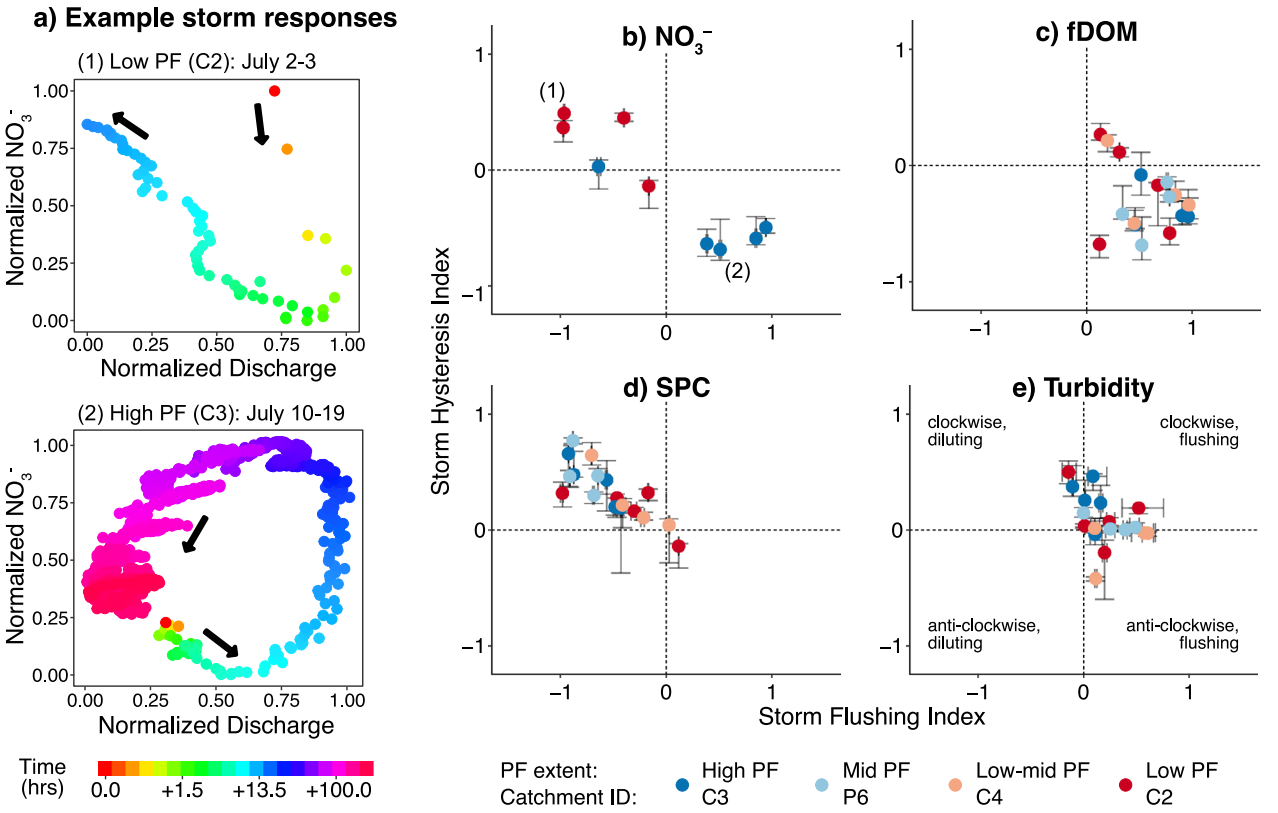

Figure 6. Concentration–discharge relationships during storms. **A** Concentration–discharge relationships for NO_3^- during two example storms (1, 2). Hysteresis index versus flushing index during all delineated storms for NO_3^- (**B**), fDOM (**C**), specific conductivity (SPC) (**D**), and turbidity (**E**). The example storm responses for NO_3^- in (**A**) are identified in (**B**). Error bars for storm hysteresis indices are bootstrapped 95% confidence intervals around the median of hysteresis indices calculated at each 2% discharge interval for each event. Error bars for storm flushing indices are bootstrapped 95% confidence intervals for the difference between the mean of solute concentration at the onset of the event and at peak discharge.

NO_3^- was coherent and consistently out-of-phase with GPP, with NO_3^- following GPP in both the high- and low-permafrost catchments (Figure 7C–D). During these periods, GPP peaked at ~ 14:00, a few hours prior to NO_3^- minima, consistent with predicted effects of in-stream N uptake (Table 1: H6). Wavelet power spectra indicated no diel pattern of variation in fDOM concentrations (Figure S4).

Discussion

Rapid climate warming at high latitudes is thawing permafrost, which in turn is altering cycling of carbon and nitrogen, elements that directly and indirectly participate in feedbacks to climate warming (Wolken and others 2011; Schuur and others 2015; Salmon and others 2016). We identified indicators of linked permafrost and ecological dynamics using multi-scale statistical approaches to compare daily to seasonal temporal patterns in stream chemistry of boreal catchments that vary in spatial extent of permafrost. We observed patterns consistent with shallow, seasonally dynamic flowpaths in a catchment with high-permafrost extent, including a seasonal increase in NO_3^- concentration and flushing of NO_3^- during storms. In contrast, dilution of NO_3^- during storms and lack of seasonal trends in a low-permafrost catchment was indicative of drainage by deep flowpaths. Overall, seasonally dynamic flowpaths and contrasting solute storage produced distinct temporal patterns in stream chemistry among catchments varying in spatial extent of permafrost that can be used to monitor ecosystem change.

Solute Export Reflects Catchment State

Contrasts in the specific yields of NO_3^- and fDOM from catchments varying in permafrost extent (Figure 2) reflected different sizes of solute pools accessible to hydrologic flowpaths. Specifically,

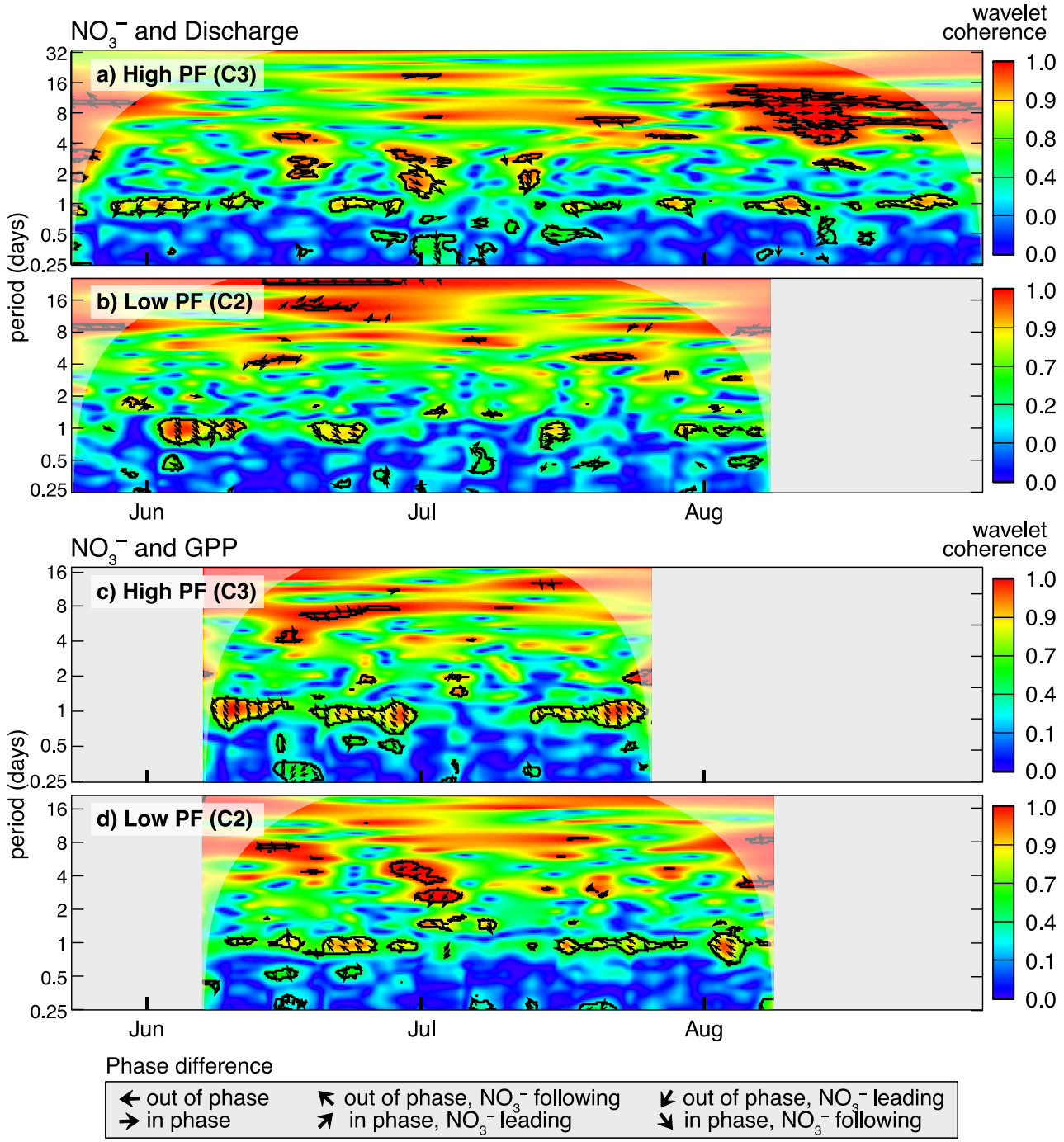

Figure 7. Wavelet coherence of NO_3^- concentration with discharge (**A**–**B**) and gross primary productivity (GPP) (**C**–**D**) in streams draining high-permafrost (**A**, **C**) and low-permafrost (PF) (**B**, **D**) catchments. Black lines indicate significant coherence ($p < 0.017$), and shading denotes areas outside the cone of influence. Colors for coherence levels are set by quantiles to provide an even color distribution. Arrows indicate the phase difference between the time series.

greater yield of NO_3^- and smaller yields of fDOM from the low- and low-mid-permafrost catchments compared to high- and mid-permafrost catchments indicated flowpaths that traversed deeper soils of greater inorganic N and lower OM content (Harden and others 2012; Melvin and others 2015). Previous studies documented similar patterns in the same study catchments (Petrone and others 2006; Balcarczyk and others 2009), and high-frequency data further revealed variance in these general

patterns due to storms (Figure 2). In addition, the mid-permafrost catchment that burned in a wildfire 13 years prior to this study exported more fDOM than all other catchments, on average (Figure 2). This contrasts with a decline in DOM export observed following the fire (Betts and Jones 2009) and indicates recovery of OM pools connected to the stream in the decade following fire.

Interactions of Hydrologic Flowpaths with Solute Sources

Seasonal-scale patterns in solute chemistry supported the hypothesis that flowpaths in permafrost-influenced catchments intersect deeper soils as the thaw season progresses (H1). Specifically, a significant increase in NO_3^- concentration in the high-permafrost catchment suggested seasonal changes in flowpath depth, whereas no trend in a low-permafrost catchment reflected the dominance of deep groundwater supporting streamflow there (Bolton and others 2004). Importantly, the trends reported here are robust to type I errors caused by features of autoregressive data (Kirchner and Neal 2013) because stream chemistry was modeled as an autoregressive process in the models we applied to estimate trends.

Several mechanisms might have contributed to the observed increase in NO_3^- concentration at a seasonal timescale, including lower biological N demand or greater rate of nitrification at depth (Harms and Jones 2012; Melvin and others 2015), increased rates of N mineralization and nitrification as soils warm (Klingensmith and Van Cleve 1993), or increasing contribution of NO_3^--rich groundwater that occurs in the region (Verplanck and others 2003). High biotic demand for N likely limits hydrologic export of N mineralized under seasonal warming (McFarland and others 2002; Lavoie and others 2011) and sustained export of fDOM from the high-permafrost catchment throughout the monitoring period (Figure 3) suggests that major flowpath contributions to streamflow likely remained within a relatively shallow active layer, rather than incurring substantial input from deep groundwater. Thus, we conclude that downward migration of shallow flowpaths is responsible for the observed season-length trend in NO_3^- concentration. This temporal trend is complementary to a positive correlation of active layer depth with NO_3^- concentration previously documented in streams across Interior Alaska (Harms and others 2016). The seasonal rate of NO_3^- increase estimated here provides a baseline against which to assess effects of continued warming, fire, or changes in precipitation regime on deepening of the active layer.

A large sustained increase in NO_3^-, fDOM, and discharge that was accompanied by a decline in SPC in the high- and mid-permafrost catchments indicated rapid activation of hydrologic flowpaths in August (Figure 2). This unexpected step-change was associated with prolonged precipitation in late summer, which can cause rapid transport of water and solutes along the permafrost boundary as well as rapid thaw of frozen soils (Koch and others 2013; James and others 2019; Douglas and others 2020) and therefore could reflect mobilization of NO_3^- from mineral or previously frozen soils. However, the concurrent flushing of fDOM and decline in SPC do not support deepening of flowpaths as the origin of the step-change because OM content declines and ions contributing to SPC increase with soil depth (Kokelj and Burn 2005; Keller and others 2007; Gough and others 2008; Ping and others 2010). Neither was precipitation the likely source of increased NO_3^- observed in the stream because $\delta^{18}O_{NO3}$ did not reflect the enriched values characteristic of atmospheric deposition (Kendall and others 2007) and $\delta^{18}O_{H2O}$ also did not shift toward heavier values more similar to rain following the step-change (Figure 4).

We hypothesize that sustained precipitation enhanced lateral hydrologic connectivity and that solutes mobilized from within the active layer caused the observed step-change in solute concentrations and discharge. The isotopic composition of NO_3^- became more enriched in the catchments where the step-change occurred, suggesting that it was derived from a different source, or that precipitation and/or transport stimulated N processing. Isotopic enrichment of NO_3^- occurs during denitrification, though increased denitrification is inconsistent with the observed increase in NO_3^- concentration. Instead, an increase in $\delta^{18}O_{NO3}$ that remained greater than $\delta^{18}O_{H2O}$ of water sources within the catchment suggested export of recently nitrified NO_3^- that had not yet undergone complete exchange of $\delta^{18}O$ with local water (Boshers and Granger 2019). Seasonal decline in terrestrial evapotranspiration might have additionally contributed to enhanced lateral hydrologic connectivity and solute mobilization during this time by raising the water table and decreasing plant N uptake (Yi and others 2009; Iwata and others 2012). Hillslope tracer studies in the nearby Nome Creek headwater catchment similarly found that shallow subsurface storage zones are rapidly flushed during large rain events (Koch and others 2017), and smaller step changes in NO_3^- concentration fol-

lowed late summer and early autumn rain events in an adjacent, larger river (Douglas and others 2013), suggesting that solute dynamics of headwater streams might propagate to larger rivers. The absence of a step-change in the low- and low-mid-permafrost catchments underscored the role of infiltration and deep drainage in structuring hydrology and biogeochemistry in boreal catchments where permafrost is absent.

Storms mobilized solutes and activated flowpaths, revealing contrasts in solute stores (Table 1: H2) and depth of dominant flowpaths (Table 1: H3) among catchments varying in spatial extent of permafrost. Specifically, storms caused flushing of NO_3^- and fDOM from the high-permafrost catchment, but dilution of NO_3^- and smaller flushes of fDOM in the low-permafrost catchment (Figure 6). Flushing of NO_3^- on the falling limb of storms in the high-permafrost catchment suggests that NO_3^- was delivered to the stream from distal locations in the catchment. A positive correlation of daily mean NO_3^- concentration with the previous day's precipitation in the high-permafrost catchment (Figure 5) corroborates the notion of longer-range transport of NO_3^- delivered to the stream on the falling limbs of storms. Together, these patterns underscore the role of permafrost in maintaining shallow flowpaths that connect soils to streams. In contrast, dilution and clockwise hysteresis of NO_3^- in the low-permafrost catchment during most storms was counter to our prediction that larger stores of NO_3^- there would generate flushing during storms (Table 1: H2-P2c). Dilution of the NO_3^--rich groundwater that supports baseflow likely occurred when storms increased flow through shallow flowpaths, such as the NO_3^--depleted soil water present in the riparian zone (Rinehart and others 2015). This pattern resembles storm responses observed in agricultural catchments encompassing NO_3^--enriched groundwater (Dupas and others 2019; Lloyd and others 2016). Simultaneous flushing of fDOM and turbidity in the low-permafrost catchment is consistent with activation of shallow flowpaths during storms. Smaller flushes of fDOM in the low- and mid-low-permafrost catchments (Figure 3) supported our expectation of smaller DOM stores there (Table 1: H2-P2b), and instances of clockwise hysteresis of fDOM in these catchments (Figure 6C) indicated that DOM supplies were sometimes exhausted during storms (Williams, 1989). Overall, however, patterns on the timescale of storms emphasized that the distribution of solute supplies relative to locations of dominant flowpaths, rather than differences in total C and N stocks in soils, influences the biogeochemical signals of permafrost observable in streams.

Biotic Influence on Temporal Variation in Stream Chemistry

Both potential growth of terrestrial vegetation (Table 1: H4–H5) and in-stream metabolism (Table 1: H6) covaried with solute concentrations in streams, though these effects were secondary to the influence of precipitation. The significant negative correlation of NO_3^- concentration with conditions favorable to terrestrial vegetation productivity (GDU) at a daily resolution (Figure 5) suggests a potential effect of biota on N export within both the high- and low-permafrost catchments, a pattern also observed in other forested catchments (Pardo and others 1995; Lucas and others 2016). GDU peaked in early July and declined by late summer, making it unlikely that this effect was related to the season-long increase in NO_3^- observed in the high-permafrost catchment. Wavelet transforms also revealed coherence in oscillations of NO_3^- concentration and discharge at a diel timescale (Figure 7), which might occur due to the effects of terrestrial evapotranspiration on water table elevation (Flewelling and others 2013; Schwab and others 2016). A higher water table enhances capacity for denitrification in the riparian zone (Harms and Jones 2012), whereas oxygenated soils above the water table might support nitrification (Duncan and others 2015). However, this mechanism is plausible only in the high-permafrost catchment early in the thaw season, when daily peaks in NO_3^- concentration occurred when discharge was low (Figure 7). Later in the thaw season, and throughout the record in the low-permafrost catchment, NO_3^- and discharge oscillated synchronously on a diel timescale, or peak daily NO_3^- concentration followed peak daily discharge, which is counter to expectations resulting from fluctuation of the water table, but consistent with N uptake by either in-stream or terrestrial biota. Negative coherence in oscillations of NO_3^- and in-stream GPP at a diel timescale in both catchments (Figure 7) as well as a negative correlation of daily in-stream GPP with NO_3^- concentration in the high-permafrost stream (Figure S2) further suggested that stream biota contributed to diel variation in NO_3^- concentration. Lack of diel variation in fDOM and inconsistent or nonsignificant correlations of either solute with daily max PAR suggest that in-stream photodegradation did not play a major role in DOM processing and was

not coupled to diel NO_3^- variation, as expected in these narrow well-shaded streams.

Implications

Permafrost generated biogeochemical signals that were observable as multi-scale temporal patterns in solute chemistry of headwater streams. Distinct signals of spatially extensive permafrost included seasonal trends, responsiveness to precipitation, counterclockwise hysteresis of concentration–discharge relationships during storms, and increasing influence of biota on diel oscillations through the growing season. Importantly, biogeochemical signals observed in streams resulted from interaction of permafrost with hydrologic flowpaths contributing to streamflow. Quantitative metrics describing these signals could be applied to detect degradation of permafrost at catchment scales, which is occurring due to climate warming, fire, and increased precipitation (Douglas and others 2020; Brown and others 2015).

Further, dominance of precipitation as a driver of catchment biogeochemistry in permafrost-influenced boreal headwaters, as demonstrated in this study, portends significant changes to solute export because precipitation is expected to become more variable at high latitudes (Bintanja and others 2020). Based on the patterns observed here, we predict that increased variation in precipitation will generate an initial increase in temporal variability of solute export, followed by a decrease in variability as permafrost thaw deepens hydrologic flowpaths. In particular, a shift toward clockwise hysteresis of concentration–discharge relationships during storms, decreased discharge and solute responses to storms, and increase in mean NO_3^- or decreased fDOM concentrations are expected indicators of deepening hydrologic flowpaths that accompany permafrost loss.

ACKNOWLEDGEMENTS

We thank Audrey Krehlik and Margaret Zahrah for their contributions to data collection. Funding was provided by the Department of Defense Strategic Environmental Research and Development Program (RC-2507 to TKH & TAD); the Bonanza Creek Long-Term Ecological Research Program, supported by the National Science Foundation (DEB-1636476) and by the USDA Forest Service, Pacific Northwest Research Station (RJVA-PNW-01-JV-11261952-231); and a Pathfinder Grant from the Consortium of Universities for the Advancement of Hydrologic Science, Inc. (to PR).

DATA AVAILABILITY

URL for applicable data: https://doi.org/10.6073/pasta/f8471eaea9705f4753b510829895a8e3

REFERENCES

Alexander HD, Mack MC. 2016. A Canopy Shift in Interior Alaskan Boreal Forests: Consequences for Above- and Belowground Carbon and Nitrogen Pools during Post-fire Succession. Ecosystems 19:98–114.

Balcarczyk KL, Jones JB, Jaffé R, Maie N. 2009. Stream dissolved organic matter bioavailability and composition in watersheds underlain with discontinuous permafrost. Biogeochemistry 94:255–270.

Bernhardt ES, Likens GE, Hall RO, Buso DC, Fisher SG, Burton TM, Meyer JL, McDowell WH, Mayer MS, Bowden WB, Findlay SEG, Macneale KH, Stelzer RS, Lowe WH. 2005. Can't See the Forest for the Stream? The capacity of instream processing to modify terrestrial nitrogen exports. Bioscience 52:219–230.

Betts EF, Jones JB. 2009. Impact of Wildfire on Stream Nutrient Chemistry and Ecosystem Metabolism in Boreal Forest Catchments of Interior Alaska. Arctic Antarct Alpine Res 41:407–417.

Bintanja R, van der Wiel K, van der Linden EC, Reusen J, Bogerd L, Krikken F, Selten FM. 2020. Strong future increases in Arctic precipitation variability linked to poleward moisture transport. Sci Adv 6:eaax869.

Brown DRN, Jorgenson MT, Douglas TA, Romanovsky V, Kielland K, Euskirchen E. 2015. Interactive effects of wildfire and climate on permafrost degradation in Alaskan lowland forests. J Geophys Res Biogeosci 120:8.

Bolton W, Hinzman L, Yoshikawa K. 2004. Water balance dynamics of three small catchments in a Sub-Arctic boreal forest. IAHS-AISH Publication:213–223.

Boshers DS, Granger J. 2019. Constraining the oxygen isotopic composition of nitrate produced by nitrification. Environ Sci Technol 53:1206–1216.

Brookshire E, Valett HM, Gerber S. 2009. Maintenance of terrestrial nutrient loss signatures during in-stream transport. Ecology 90:293–299.

Bugmann HKM, Wullschleger SD, Price DT, Ogle K, Clark DF, Solomon AM. 2001. Comparing the performance of forest gap models in North America. Climatic Change 51:349–388.

Burns DA, Pellerin BA, Miller MP, Capel PD, Tesoriero AJ, Duncan JM. 2019. Monitoring the riverine pulse: Applying high-frequency nitrate data to advance integrative understanding of biogeochemical and hydrological processes. Wiley Interdiscip Rev 6:e1348.

Casciotti KL, Sigman DM, Hastings MG, Böhlke JK, Hilkert A. 2002. Measurement of the oxygen isotopic composition of nitrate in seawater and freshwater using the denitrifier method. Anal Chem 74:4905–4912.

Czikowsky MJ, Fitzjarrald DR. 2004. Evidence of seasonal changes in evapotranspiration in eastern U.S. hydrological records. J Hydrometeorol 5:974–988.

Douglas TA, Blum JD, Guo L, Keller K, Gleason JD. 2013. Hydrogeochemistry of seasonal flow regimes in the Chena River, a subarctic watershed draining discontinuous permafrost in interior Alaska (USA). Chem Geol 335:48–62.

Douglas TA, Turetsky MR, Koven CD. 2020. Increased rainfall stimulates permafrost thaw across a variety of Alaskan ecosystems. Nat Climate Atmos Sci 3:28.

Downing BD, Pellerin BA, Bergamaschi BA, Saraceno JF, Kraus TEC. 2012. Seeing the light: The effects of particles, dissolved materials, and temperature on in situ measurements of DOM fluorescence in rivers and streams. Limnol Oceanogr Methods 10:767–775.

Duncan JM, Band LE, Groffman PM, Bernhardt ES. 2015. Mechanisms driving the seasonality of catchment scale nitrate export: Evidence for riparian ecohydrologic controls. Water Resour Res 51:3982–3997.

Dupas R, Abbott BW, Minaudo C, Fovet O. 2019. Distribution of landscape units within catchments influences nutrient export dynamics. Frontiers Environ Sci 7:43.

Flewelling SA, Hornberger GM, Herman JS, Mills AL, Robertson WM. 2013. Diel patterns in coastal-stream nitrate concentrations linked to evapotranspiration in the riparian zone of a low-relief, agricultural catchment. Hydrol Processes 28:2150–2158.

Fork ML, Sponseller RA, Laudon H. 2020. Changing source-transport dynamics drive differential browning trends in a boreal stream network. Water Resour Res 56:2.

Fuka DR, Walter MT, Archibald JA, Steenhuis TS, Easton ZM. 2018. EcoHydRology: A Community Modeling Foundation for Eco-Hydrology. R package version 0.4.12.1.

Giling D, Bond N. 2020. BASEmetab: Estimate Single-station Whole-stream Metabolic Rates from Diel Dissolved Oxygen Curves. R package version 3.0.

Gough LP, Crock JG, Wang B, Day WC, Eberl DD, Sanzolone RF, Lamothe PJ. 2008. Substrate Geochemistry and Soil Development in Boreal Forest and Tundra Ecosystems in the Yukon-Tanana Upland and Seward Peninsula, Alaska. USGS: pubs.er.usgs.gov/usgspubs/sir/sir20085010.

Grace MR, Giling DP, Hladyz S, Caron V, Thompson RM, Mac Nally R. 2015. Fast processing of diel oxygen curves: Estimating stream metabolism with base (BAyesian single-station estimation). Limnol Oceanogr Methods 13:103–114.

Hall RO, Tank JL, Baker MA, Rosi-Marshall EJ, Hotchkiss ER. 2016. Metabolism, Gas Exchange, and Carbon Spiraling in Rivers. Ecosystems 19:73–86.

Harden JW, Koven CD, Ping CL, Hugelius G, David McGuire A, Camill P, Jorgenson T, Kuhry P, Michaelson GJ, O'Donnell JA, Schuur EAG, Tarnocai C, Johnson K, Grosse G. 2012. Field information links permafrost carbon to physical vulnerabilities of thawing. Geophys Res Lett 39:1–6.

Harms TK, Jones JB. 2012. Thaw depth determines reaction and transport of inorganic nitrogen in valley bottom permafrost soils. Global Change Biol 18:2958–2968.

Harms TK, Edmonds JW, Genet H, Creed IF, Aldred D, Balser A, Jones JB. 2016. Catchment influence on nitrate and dissolved organic matter in Alaskan streams across a latitudinal gradient. J Geophys Res Biogeosci 121:350–369.

Haugen RK, Slaughter CW, Howe KE, Dingman SL. 1982. Hydrology and climatology of the Caribou-Poker Creek Research Watershed, Alaska.

Hinzman LD, Fukuda M, Sandberg DV, Chapin FS, Dash D. 2003. FROSTFIRE: An experimental approach to predicting the climate feedbacks from the changing boreal fire regime. J Geophys Res 108:1996–2001.

Holmes EE, Ward EJ, Scheuerell M, Wills K. 2018. Package 'MARSS'. R package version 3.10.12. Available at https://cran.r-project.org/web/packages/MARSS/MARSS.pdf.

Iwata H, Harazono Y, Ueyama M. 2012. The role of permafrost in water exchange of a black spruce forest in Interior Alaska. Agric Forest Meteorol 161:107–115.

James SR, Knox HA, Abbott RE, Panning MP, Screaton EJ. 2019. Insights Into Permafrost and Seasonal Active-Layer Dynamics From Ambient Seismic Noise Monitoring. J Geophys Res Earth Surface 124:1798–1816.

Johnstone JF, Chapin FS, Hollingsworth TN, Mack MC, Romanovsky V, Turetsky M. 2010. Fire, climate change, and forest resilience in interior Alaska. Can J Forest Res 40:1302–1312.

Jones CS, Wang B, Schilling KE, Chan K. 2017. Nitrate transport and supply limitations quantified using high-frequency stream monitoring and turning point analysis. J Hydrol 549:581–591.

Jorgenson MT, Romanovsky V, Harden J, Shur Y, O'Donnell J, Schuur EAG, Kanevskiy M, Marchenko S. 2010. Resilience and vulnerability of permafrost to climate change. Can J Forest Res 40:1219–1236.

Keller K, Blum JD, Kling GW. 2007. Geochemistry of soils and streams on surfaces of varying ages in arctic Alaska. Arctic Antarct Alpine Res 39:84–98.

Keller K, Blum JD, Kling GW. 2010. Stream geochemistry as an indicator of increasing permafrost thaw depth in an arctic watershed. Chem Geol 273:76–81.

Kendall C, Elliott EM, Wankel SD. 2007. Tracing anthropogenic inputs of nitrogen to ecosystems. Stable Isotopes Ecol Environ Sci 2:375–449.

Klingensmith K, Van Cleve K. 1993. Patterns of nitrogen mineralization and nitrification in floodplain successional soils along the Tanana River, Interior Alaska. Can J Forest Res 23:964–969.

Koch JC, Ewing SA, Striegl R, McKnight DM. 2013. Rapid runoff via shallow throughflow and deeper preferential flow in a boreal catchment underlain by frozen silt (Alaska, USA). Hydrogeol J 21:93–106.

Koch JC, Kikuchi CP, Wickland KP, Schuster P. 2014. Runoff sources and flow paths in a partially burned, upland boreal catchment underlain by permafrost. Water Resour Res 50:8141–8158.

Koch JC, Toohey RC, Reeves DM. 2017. Tracer-based evidence of heterogeneity in subsurface flow and storage within a boreal hillslope. Hydrol Processes 31:2453–2463.

Kokelj SV, Burn CR. 2005. Geochemistry of the active layer and near-surface permafrost, Mackenzie delta region, Canada. Can J Earth Sci 42:37–48.

Kirchner JW, Feng X, Neal C, Robson AJ. 2004. The fine structure of water-quality dynamics: The (high-frequency) wave of the future. Hydrolo Process 18:1353–1359.

Kirchner JW, Neal C. 2013. Universal fractal scaling in stream chemistry and its implications for solute transport and water quality trend detection. Proc Natl Acad Sci 110:12213–12218.

Lavoie M, Mack MC, Schuur EAG. 2011. Effects of elevated nitrogen and temperature on carbon and nitrogen dynamics in Alaskan arctic and boreal soils. J Geophys Res Biogeosci 116:1–14.

Likens GE, Bormann FH, Johnson NM, Fisher D, Robert S. 1970. Effects of Forest Cutting and Herbicide Treatment on Nutrient Budgets in the Hubbard Brook Watershed-Ecosystem. Ecol Monogr 40:23–47.

Lloyd CEM, Freer JE, Johnes PJ, Collins AL. 2016. Using hysteresis analysis of high-resolution water quality monitoring data, including uncertainty, to infer controls on nutrient and sediment transfer in catchments. Sci Total Environ 543:388–404.

Lucas RW, Sponseller RA, Gundale MJ, Stendahl J, Fridman J, Högberg P, Laudon H. 2016. Long-term declines in stream and river inorganic nitrogen (N) export correspond to forest change. Ecol Appl 26:545–556.

McFarland J, Ruess R, Kielland K, Doyle A. 2002. Cycling Dynamics of NH4+ and Amino Acid Nitrogen in Soils of a Deciduous Boreal Forest Ecosystem. Ecosystems 5:775–788.

McGuire KJ, McDonnell JJ. 2006. A review and evaluation of catchment transit time modeling. J Hydrol 330:543–563.

Melvin AM, Mack MC, Johnstone JF, McGuire AD, Genet H, Schuur EA. 2015. Differences in ecosystem carbon distribution and nutrient cycling linked to forest tree species composition in a mid-successional boreal forest. Ecosystems 18:1472–1488.

Mutschlecner AE, Guerard JJ, Jones JB, Harms TK. 2018. Phosphorus Enhances Uptake of Dissolved Organic Matter in Boreal Streams. Ecosystems 21:675–688.

Nimick DA, Gammons CH, Parker SR. 2011. Diel biogeochemical processes and their effect on the aqueous chemistry of streams: A review. Chem Geol 283:3–17.

Odum HT. 1956. Primary production in flowing waters. Limnol Oceanogr 1:102–117.

Pardo LH, Driscoll CT, Likens GE. 1995. Patterns of nitrate loss from a chronosequence of clear-cut watersheds. Water Air Soil Pollut 85:1659–1664.

Petrone KC, Jones JB, Hinzman LD, Boone RD. 2006. Seasonal export of carbon, nitrogen, and major solutes from Alaskan catchments with discontinuous permafrost. J Geophys Res Biogeosci 111:1–13.

Petrone KC, Hinzman LD, Shibata H, Jones JB, Boone RD. 2007. The influence of fire and permafrost on sub-arctic stream chemistry during storms. Hydrol Process 21:423–434.

Ping CL, Michaelson GJ, Kane ES, Packee EC, Stiles CA, Swanson DK, Zaman ND. 2010. Carbon Stores and Biogeochemical Properties of Soils under Black Spruce Forest, Alaska. Soil Sci Soc Am J 74:969–978.

Rinehart AJ, Jones JB, Harms TK. 2015. Hydrologic and biogeochemical influences on carbon processing in the riparian zone of a subarctic stream. Freshwater Sci 34:222–232.

Roesch A, Schmidbauer H. 2018. WaveletComp. R package version 1.1.

Rollinson CR, Liu Y, Raiho A, Moore DJP, McLachlan J, Bishop DA, Dye A, Matthes JH, Hessl A, Hickler T, Pederson N, Poulter B, Quaife T, Schaefer K, Steinkamp J, Dietze MC. 2017. Emergent climate and CO2 sensitivities of net primary productivity in ecosystem models do not agree with empirical data in temperate forests of eastern North America. Glob Chang Biol 23:2755–2767.

Ruosteenoja K, Räisänen J, Venäläinen A, Kämäräinen M. 2016. Projections for the duration and degree days of the thermal growing season in Europe derived from CMIP5 model output. Int J Clim 36:3039–3055.

Salmon VG, Soucy P, Mauritz M, Celis G, Natali SM, Mack MC, Schuur EAG. 2016. Nitrogen availability increases in a tundra ecosystem during five years of experimental permafrost thaw. Glob Chang Biol 22:1927–1941.

Schwab M, Klaus J, Pfister L, Weiler M. 2016. Diel discharge cycles explained through viscosity fluctuations in riparian inflow. Water Resour Res 52:8744–8755.

Schuur EAG, McGuire AD, Schädel C, Grosse G, Harden JW, Hayes DJ, Hugelius G, Koven CD, Kuhry P, Lawrence DM, Natali SM, Olefeldt D, Romanovsky VE, Schaefer K, Turetsky MR, Treat CC, Vonk JE. 2015. Climate change and the permafrost carbon feedback. Nature 520:171–179.

Ueyama M, Iwata H, Harazono Y, Euskirchen ES, Oechel WC, Zona D. 2013. Growing season and spatial variations of carbon fluxes of Arctic and boreal ecosystems in Alaska (USA). Ecol Appl 23:1798–1816.

van Cleve K, Chapin FS, Dyrness CT, Viereck LA. 1991. Element Cycling in Taiga Forests: State-Factor Control. BioScience 41:78–88.

Vaughan MCH, Bowden WB, Shanley JB, Vermilyea A, Sleeper R, Gold AJ, Pradhanang SM, Inamdar SP, Levia DF, Andres AS, Birgand F, Schroth A. 2017. High-frequency dissolved organic carbon and nitrate measurements reveal differences in storm hysteresis and loading in relation to land cover and seasonality. Water Resour Res 53:5345–5363.

Verplanck PL, Mueller SH, Youcha EK, Goldfarb RJ, Sanzolone RF, McCleskey RB, Briggs PH, Roller M, Adams M, Nordstrom DK. 2003. Chemical Analyses of Ground and Surface Waters, Ester Dome, Cental Alaska, 2000–2001. U.S. Geological Survey Open-File Report 03–244 (available at https://pubs.usgs.gov/of/2003/ofr-03-244/).

Watras CJ, Hanson PC, Stacy TL, Morrison KM, Mather J, Hu YH, Milewski P. 2011. A temperature compensation method for CDOM fluorescence sensors in freshwater. Limnol Oceanogr Methods 9:296–301.

Williams GP. 1989. Sediment concentration versus water discharge during single hydrologic events. J Hydrol 111:89–106.

Wolken JM, Hollingsworth TN, Rupp TS, Chapin III FS, Trainor SF, Barrett TM, Sullivan PF, McGuire AD, Euskirchen ES, Hennon PE, Beever EA, Conn JS, Crone LK, D'Amore DV, Fresco N, Hanley TA, Kielland K, Kruse JJ, Patterson T, Schuur EAG, Verbyla DL, Yarie J. 2011. Evidence and implications of recent and projected climate change in Alaska's forest ecosystems. Ecosphere 2:art124.

Yi S, McGuire AD, Harden J, Kasischke E, Manies K, Hinzman L, Liljedahl A, Randerson J, Liu H, Romanovsky V, Marchenko S, Kim Y. 2009. Interactions between soil thermal and hydrological dynamics in the response of Alaska ecosystems to fire disturbance. J Geophys Res: Biogeosci 114:1–20.

Yoshikawa K, White DM, Hinzman LD, Goering DJ, Petrone KC, Bolton WR, Ishikawa N. 2003. Water in permafrost: Case study of aufeis and pingo hydrology in discontinuous permafrost. Proceedings of the Int. Conference on Permafrost. Zurich, Switzerland 1259–64.